European Journal of Radiology 110 (2019) 112–120

Contents lists available at ScienceDirect

European Journal of Radiology

journal homepage: www.elsevier.com/locate/ejrad

Research article

Characterization of prostate cancer using diffusion tensor imaging: A new perspective

Neda Gholizadeh[a], Peter B. Greer[b,c], John Simpson[b,c], Jim Denham[b], Peter Lau[d,e], Jason Dowling[f], Hubert Hondermarck[g], Saadallah Ramadan[a,d,*]

[a] School of Health Sciences, University of Newcastle, Callaghan, NSW, Australia
[b] Department of Radiation Oncology, Calvary Mater Hospital, Waratah, NSW, Australia
[c] School of Mathematical and Physical Sciences, University of Newcastle, Callaghan, NSW, 2308, Australia
[d] Hunter Medical Research Institute (HMRI) Imaging Centre, New Lambton Heights, NSW, Australia
[e] Department of Radiology, Calvary Mater Hospital, Waratah, NSW, Australia
[f] CSIRO Australian e-Health Research Centre, Herston, Queensland, Australia
[g] School of Biomedical Sciences and Pharmacy, University of Newcastle, Callaghan, NSW, 2308, Australia

ARTICLE INFO

Keywords:
Quantitative parameters
Diffusing tensor imaging
Prostate
Cancer

ABSTRACT

Purpose: This study is aimed at evaluating the potential role of quantitative magnetic resonance diffusion tensor imaging (DTI) and tractography parameters in the detection and characterization of peripheral zone prostate cancer with a particular attention for fiber tract density.

Materials and methods: DTI was acquired from eleven high risk, transrectal ultrasound (TRUS)-guided biopsy proven prostate cancers with perineural invasion (histological Gleason score ≥ 7) on a 3 T magnet. Twenty parameters derived from DTI were quantified in cancer and healthy regions of the prostate. In addition, fiber tract density in normal versus cancer tissues was also calculated using DTI tractography. Support vector machine with a radial basis function kernel and area under receiver operator characteristic (ROC) were used to describe and compare the diagnostic performance of combined fractional anisotropy (FA) and mean diffusivity (MD) and other statistically significant DTI parameters. Spearman correlation analysis between DTI parameters and Gleason scores was conducted.

Results: Eighteen DTI parameters yielded statistically significant differences between cancer and healthy regions (p-value < 0.05). The ROC curve of all statistically significant DTI parameters between cancer and healthy regions was higher than the area under ROC curve using FA + MD alone (95% confidence interval = 0.988, range = 0.975–1.00) vs (95% confidence interval = 0.935, range = 0.898-0.999), respectively (p-value < 0.05). Fiber tract density was also found to be higher in cancer than in healthy tissues (+38.22%, p-value = 0.010) and may be related to the increase in nerve and vascular density reported in prostate cancer. The linear and relative anisotropy were highly correlated with Gleason score (Spearman correlation factor r = 0.655, p-value = 0.001 and r = 0.667, p-value < 0.001, respectively).

Conclusions: DTI has the potential to provide imaging biomarkers in the detection and characterization of prostate cancer. Novel quantitative parameters derived from DTI and DTI tractography, including fiber tract density, support the use of DTI in the assessment of high grade prostate cancer.

1. Introduction

Prostate cancer is the most common non-cutaneous malignancy in males [1]. In clinical practice, men with elevated prostate-specific antigen (PSA) and positive digital rectal examination require transrectal ultrasound (TRUS)-guided biopsy. Perineural invasion in prostate cancer, defined as the infiltration of nerves by cancer cells, is present in approximately 50–85% of high risk prostate cancer patients [2]. The detection of perineural invasion in prostate cancer biopsies is a worrying histopathological parameter of prognostic significance along with

Abbreviations: DTI, diffusion tensor imaging; ROC, receiver operator characteristic; FA, fractional anisotropy; MD, mean diffusivity; PSA, prostate-specific antigen; DWI, diffusion weighted imaging; λ_1, axial diffusivity; RD, radial diffusivity; C_l, linear anisotropy; C_p, planar anisotropy; C_s, spherical anisotropy; AC, attenuation coefficient; RA, relative anisotropy; PZ, peripheral zone; VD, volume diffusivity; ROI, regions of interest; SVM, support vector machine; RBF, radial basis function

* Corresponding author at: Hunter Medical Research Institute, Kookaburra Circuit, New Lambton, New South Wales, 2305, Australia.
E-mail address: Saadallah.ramadan@newcastle.edu.au (S. Ramadan).

https://doi.org/10.1016/j.ejrad.2018.11.026
Received 9 September 2018; Received in revised form 19 November 2018; Accepted 21 November 2018

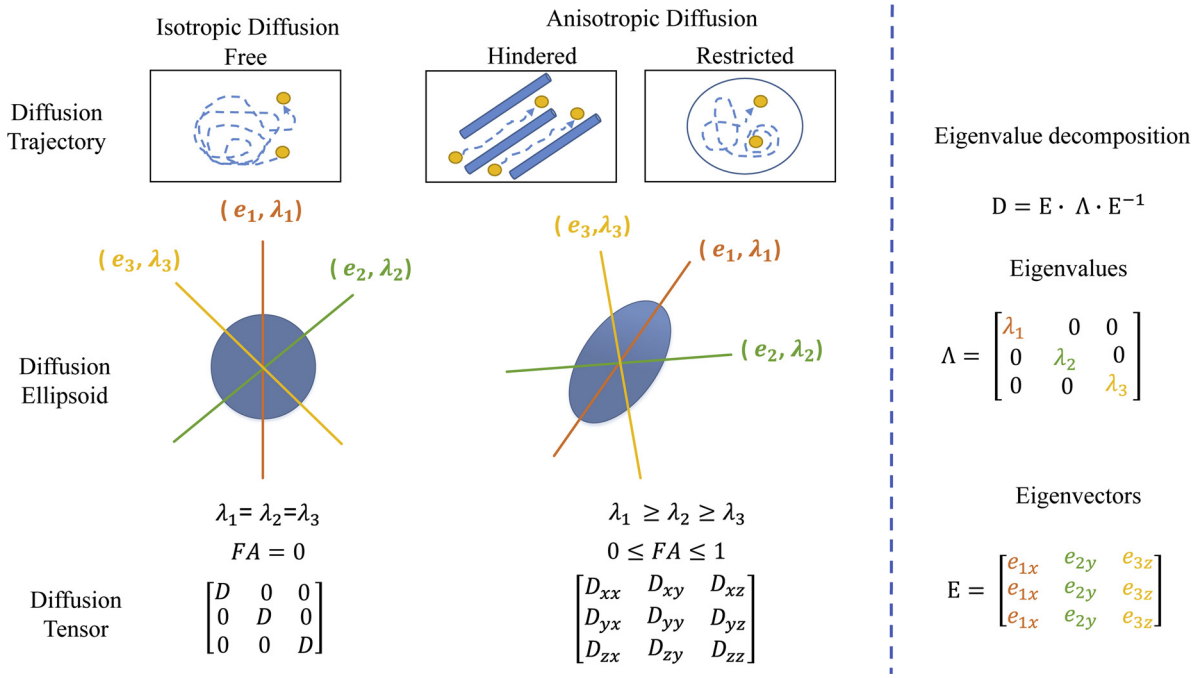

Fig. 1. Diffusion trajectory, ellipsoids and tensor for isotropic (free) and anisotropic (hindered and restricted) diffusion. In isotropic environments, water diffusion is the same in all different geometrical orientations, whereas in anisotropic environments, water diffusion is influenced by microstructures and hindrances available nearby that has the potential to direct water diffusion along certain defined trajectories, leading to different diffusion values in different directions. The diffusion tensor can be mathematically decomposed into eigenvectors (direction) and eigenvalues (magnitude).

Gleason score and clinical staging. This pathological information help physicians to treat each individual prostate cancer patient in a more precise manner. Importantly, recent evidence has unravelled the role of nerves in stimulating cancer initiation and progression [3]. In prostate cancer, the density of nerve fibers is increased in the tumor microenvironment and is associated with prostate tumor and histological grade (Gleason score) [4]. The increased presence of nerve fibers in prostate cancer is stimulated by the release of neurotrophic factors by cancer cells [5,6] which induces an angiogenic switch that fuels tumor growth and metastasis [7].

The *in vivo* association of diffusion weighted imaging (DWI) and prostate cancer pathology was determined by many dedicated studies [8]. DWI is sensitive to the thermally driven Brownian motion of water molecules in biological tissues. However, due to the complex cellular structure of biological tissues, diffusion is usually hindered or restricted (also known as anisotropic) along preferred directions depending on structural orientations of fiber-like structures, such as fascial layers, smooth muscle elastic fibers, capillaries and neural networks [9]. This leads to increased water diffusivity along these preferred directions. Diffusion tensor imaging (DTI) can characterize diffusion along multiple directions and can potentially provide anisotropic diffusion information [10], leading to the visualization of networks of pathways along which water preferentially diffuses [10]. Several studies have investigated the potential of mean diffusivity (MD) and fractional anisotropy (FA) from DTI studies in prostate cancer detection [11] and their correlation with Gleason score [12], yielding mixed results. However, other tensor metrics, including axial diffusivity (λ_1), radial diffusivity (RD), linear anisotropy (C_l), planar anisotropy (C_p), spherical anisotropy (C_s), attenuation coefficient (AC) map and relative anisotropy (RA) have also shown promise in characterizing tissue abnormalities [13]. Moreover, these measured diffusion tensor metrics can offer novel biophysical interpretation of the geometric nature of the fiber tract organization [14]. Previous studies demonstrated a significant correlation between tissue microscopic morphology and the diffusion parameters obtained noninvasively with DTI. To our knowledge, no published studies have reported the value of these parameters in the characterization of prostate cancer with similar morphology. DTI tractography reconstructs fiber tracts in three dimensions to enable visualization of tissue microstructures. Several studies have reported the wide distribution of periprostatic nerve plexus around the prostate in prostate cancer patients using DTI tractography [14,15]. However, at this stage, it is not clear if DTI fiber tractography of the prostate can provide any supporting *in vivo* evidence or agree with increased nerve fiber density in prostate cancer tissues, which warrants further investigations.

The purpose of this prospective study is to demonstrate if DTI and DTI tractography parameters can provide more details of prostate tissue microstructure to improve characterization of prostate cancer with perineural invasion.

In this study, DTI data from peripheral zone (PZ) prostate cancer patients was acquired and post-processed using specialized software. Second, twenty-one DTI metrics including novel volume diffusivity (VD), three surface diffusivities and fiber tract density were calculated, compared and analysed in cancer and healthy tissues. The diagnostic performance of DTI using quantitative DTI parameters was evaluated and compared to the conventional parameters. Finally, the correlation of DTI parameters with tumor grade (Gleason score) was evaluated.

2. Materials and methods

2.1. Quantitative DTI maps

DTI is an extension of DWI where water diffusion directional dependence can be evaluated in at least six directions. DTI is a tensor and provides extra structural information about the magnitude and anisotropy of water diffusion in tissues. This tensor is a 3 × 3 positive symmetric matrix of vectors that can be mathematically decomposed into eigenvectors (e_1, e_2 and e_3) and eigenvalues (λ_1, λ_2 and λ_3). Fig. 1 represents the basis of the most common quantitative DTI measurements.

The most common prostate DTI measures are the MD and FA [16,17]. However, DTI can give more information regarding preferential diffusion of water and biophysical characteristics of prostate

Table 1
Clinical information of the recruited peripheral zone prostate cancer patients.

	Mean ± SD*	Range
Age(years)	71.4 ± 9.2	54 – 87
PSA (ng/mL)	16.6 ± 12.9	1.3 – 37.2
Biopsy Gleason score	**Number of patients (total = 11)**	**%**
4 + 3	6	54.5
4 + 5	5	44.5

* SD: Standard deviation.

tissue. In this study, multiple quantitative anisotropic and diffusivity parameters of DTI were evaluated, and these can be described briefly as follows:

Anisotropy parameters: Fractional anisotropy (FA), relative anisotropy (RA), volume ratio (VR), linear (C_l), planar (C_p) and spherical (C_s) anisotropies, attenuation coefficient (AC) as well as anisotropy mode (Mode).

Diffusivity parameters: Mean diffusivity (MD), axial diffusivity (λ_1), two orthogonal diffusivities to λ_1 (λ_2 *and* λ_3) and four radial diffusivities (RD, $\lambda_1 - \lambda_2$, $\lambda_1 - \lambda_3$ and $\lambda_2 - \lambda_3$), [10] in addition to novel DTI parameters, volume diffusivity (VD = $\lambda_1\lambda_2\lambda_3$) and surface diffusivities ($S_{e_1e_2} = \lambda_1\lambda_2$, $S_{e_1e_3} = \lambda_1\lambda_3$ *and* $S_{e_2e_3} = \lambda_2\lambda_3$).

Furthermore, this tensor provides information about diffusion and diffusion barriers e.g. muscle, vascular structures and nerves and can give an insight into total fiber tracts and microstructures. The principle direction of diffusion can be followed in each voxel to reconstruct a path through the image which is termed “tractography” or “fiber tracking”. Many such tractographic streamlines can be displayed to form virtual reconstructions, which may provide a reasonable approximation of macroscopic anatomical fiber bundles. The number of fiber tracts derived from DTI tractography per unit volume, known as ‘fiber tract density’, was also evaluated in this study in both cancer and healthy regions of the prostate.

2.2. Patients and patient preparation

Informed and written consent was obtained from all patients to participate in this prospective study which was approved by local institutional human ethics review board. All patients underwent 16-core (S16C) 8 zones TRUS guided biopsy at least six weeks before the MRI scan. A total of twelve high risk, TRUS guided biopsy-proven PZ prostate cancer patients with perineural invasion were recruited in this study between August 2016 and May 2018. One patient with Parkinson disease was excluded due to image distortion artefacts, leaving eleven patients. Prostatectomy was not carried out in any patient in this study.

The inclusion criteria were: (i) patients with (TRUS) biopsy-proven prostate cancer with perineural invasion and with complete clinical data, (ii) patients without any contraindication of using the MRI and (iii) at least six weeks after the biopsy. The exclusion criteria were: (i) data with insufficient quality, (ii) prior PCa treatment, (iii) presence of hip prosthesis, (iv) pelvic nodal involvement and (v) men with mental impairment/intellectual impairment would have difficulty giving informed consent to the study.

All patients underwent contrast-free T2 weighted imaging (T2WI), DWI and DTI. One main limitation of prostate DTI is the sensitivity to motion and prostate movement, such as air-tissue interfaces [18]. In an attempt to overcome this limitation, all patients were restricted to a low fiber diet 24 h before scan and were asked to empty bladder and received a rectal laxative (Microlax®, Sanofi-Winthrop, Colombiers, France) before MRI imaging sessions.

2.3. MRI protocol

The MR images were obtained with a 3 T Skyra scanner (Siemens Healthineers, Erlangen, Germany, maximum gradient amplitude (single axis): 45 m T/m, minimum gradient rise time: 225 μs, maximum gradient slew rate: 200 T/m/sec) using an external 18-channel phase array coil (Siemens Healthineers, Erlangen, Germany). A two-dimensional turbo spin echo (TSE) T2WI of the prostate was performed axially with the following parameters: repetition time (TR): 1400 ms; echo time (TE): 96 ms; number of averages: 3; flip angle: 135°; slice thickness: 4 mm; no gap; field of view (FOV): 200 mm; and total acquisition time: 3.45 min.

DWI was obtained using single shot echo planar imaging (EPI) and the following parameters: TR: 4600 ms, TE: 65 ms; slice thickness:

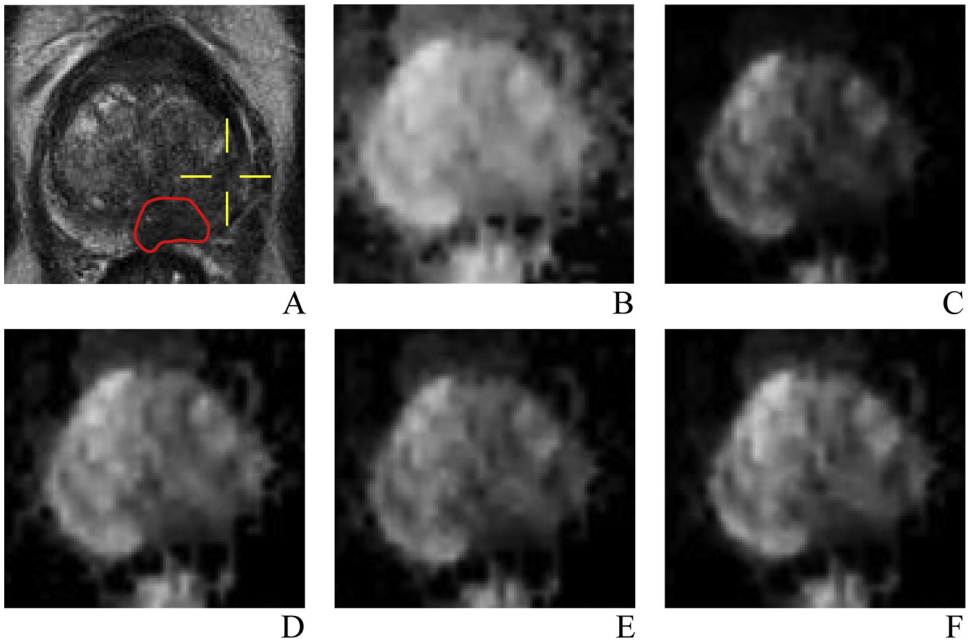

Fig. 2. A) T2WI of a 66 year old man with a PSA value of 21.0 ng/mL and 4 + 3 Gleason score peripheral zone prostate cancer in the left PZ with outlined cancer region of interest (ROI) (red line) and marked suspicious area (yellow lines), B) mean diffusivity (MD), C) volume diffusivity (VD), three surface diffusivities D) $S_{e_1e_2}$, E) $S_{e_1e_3}$, and F) $S_{e_2e_3}$ DTI maps. Visual inspection shows more hypo-intense regions in VD, $S_{e_1e_2}$, $S_{e_1e_3}$ and $S_{e_2e_3}$ than corresponding T2WI (A) and MD map (B).

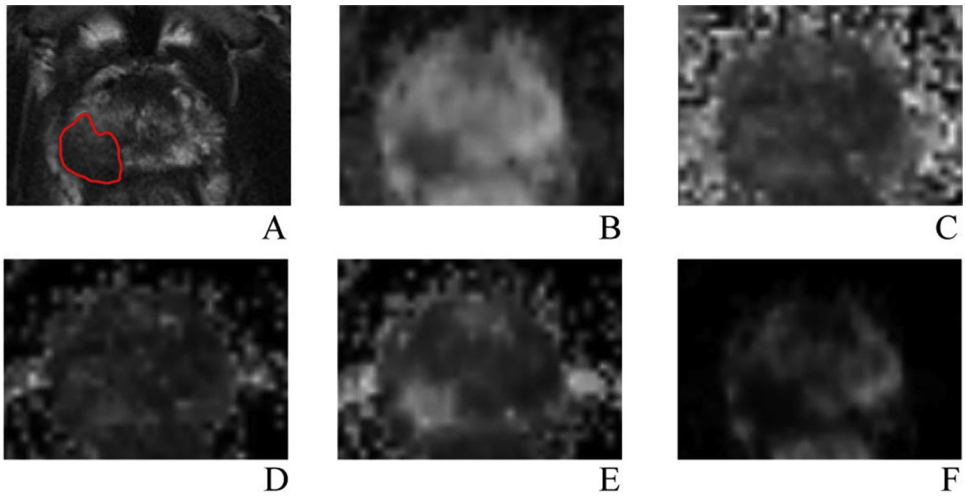

Fig. 3. A) T2WI of a 71-year-old man with a PSA value of 11.6 ng/mL and 4 + 3 Gleason score peripheral zone prostate cancer in right peripheral zone (PZ) with outlined cancer region of interest (ROI) (red line), B) mean diffusivity (MD), C) fractional anisotropy (FA), D) relative anisotropy (RA), E) volume diffusivity (VD) and F) attenuation coefficient (AC) DTI maps. Different DTI maps offer subtle and different types of information about microstructure of tissue compared to T2WI (A) and MD map (B).

Table 2
Analysis of various DTI parameters for cancer and healthy tissues. Cancer ROIs were obtained from combined cancer Gleason scores (4 + 3 and 4 + 5).

	Healthy Mean ± SD	Cancer Mean ± SD	P-value	Cut-off
DWI Feature				
ADC	1.60 ± 0.12	1.01 ± 0.18	< 0.001	1.32
DTI Feature				
FA	0.22 ± 0.04	0.31 ± 0.09	0.006	0.27
RA	0.13 ± 0.02	0.17 ± 0.02	0.001	0.15
VR	0.86 ± 0.04	0.82 ± 0.05	0.024	0.85
C_l	0.07 ± 0.01	0.10 ± 0.01	< 0.001	0.09
C_p	0.16 ± 0.02	0.20 ± 0.02	< 0.001	0.18
C_s	0.77 ± 0.09	0.70 ± 0.07	0.005	0.76
AC	0.13 ± 0.02	0.26 ± 0.08	< 0.001	0.18
Mode	0.05 ± 0.12	0.08 ± 0.14	0.372	0.07
MD ($\times 10^{-3}$ mm^2/s)	1.51 ± 0.23	0.99 ± 0.27	< 0.001	1.21
λ_1($\times 10^{-3}$ mm^2/sec)	1.75 ± 0.29	1.24 ± 0.30	< 0.001	1.44
λ_2($\times 10^{-3}$ mm^2/sec)	1.42 ± 0.26	0.96 ± 0.27	< 0.001	1.15
λ_3($\times 10^{-3}$ mm^2/sec)	1.03 ± 0.18	0.67 ± 0.20	< 0.001	0.78
RD ($\times 10^{-3}$ mm^2/sec)	1.23 ± 0.22	0.82 ± 0.23	< 0.001	0.98
$\lambda_1 - \lambda_2$($\times 10^{-3}$ mm^2/sec)	0.24 ± 0.02	0.20 ± 0.03	0.011	0.22
$\lambda_1 - \lambda_3$($\times 10^{-3}$ mm^2/sec)	0.51 ± 0.05	0.44 ± 0.05	0.010	0.48
$\lambda_2 - \lambda_3$($\times 10^{-3}$ mm^2/sec)	0.21 ± 0.02	0.19 ± 0.02	0.059	0.20
VD ($\times 10^{-3}$ mm^2/sec)^3	2.97 ± 1.48	1.04 ± 0.68	< 0.001	1.63
$S_{e_1e_2}$($\times 10^{-3}$ mm^2/sec)^2	2.62 ± 0.90	1.30 ± 0.72	< 0.001	1.80
$S_{e_1e_3}$($\times 10^{-3}$ mm^2/sec)^2	1.90 ± 0.60	0.90 ± 0.52	< 0.001	1.25
$S_{e_2e_3}$($\times 10^{-3}$ mm^2/sec)^2	1.58 ± 0.53	0.71 ± 0.44	< 0.001	0.98
Fiber tract density (per cm^3)	19.44 ± 4.39	26.87 ± 6.80	0.010	22.04

Fractional anisotropy (FA), relative anisotropy (RA), volume ratio (VR), linear anisotropy (C_l), planar anisotropy (C_p), spherical anisotropy (C_s), attenuation coefficient (AC), anisotropy mode (Mode), mean diffusivity (MD), axial diffusivity (λ_1), two orthogonal diffusivities to λ_1 (λ_2 *and* λ_3), four radial diffusivities (RD, $\lambda_1 - \lambda_2$, $\lambda_1 - \lambda_3$ and $\lambda_2 - \lambda_3$), volume diffusivity (VD = $\lambda_1\lambda_2\lambda_3$) and surface diffusivities ($S_{e_1e_2} = \lambda_1\lambda_2$, $S_{e_1e_3} = \lambda_1\lambda_3$ *and* $S_{e_2e_3} = \lambda_2\lambda_3$).

4 mm; no gap; FOV: 260 × 260 mm^2 and b-values of 50, 400 and 800 s/mm^2 and total acquisition time: 4.19 min.

Axial DTI were obtained using a fat suppressed single shot echo planar imaging sequence. The MRI signal was sensitized to diffusion by application of a pair of bipolar trapezoidal gradient pulses with duration of effective δ (38.550 ms) and effective diffusion time Δ (48.810 ms) in 30 equally and spherically distributed directions [19] with a matrix of 152 × 152; TR: 11,300 ms; TE: 101 ms; number of averages: 1; slice thickness: 4 mm; no gap; FOV: 260 × 260 mm^2; and b-values of 0 and 1600s/mm^2 [20]. The DTI total acquisition time was 6.62 min.

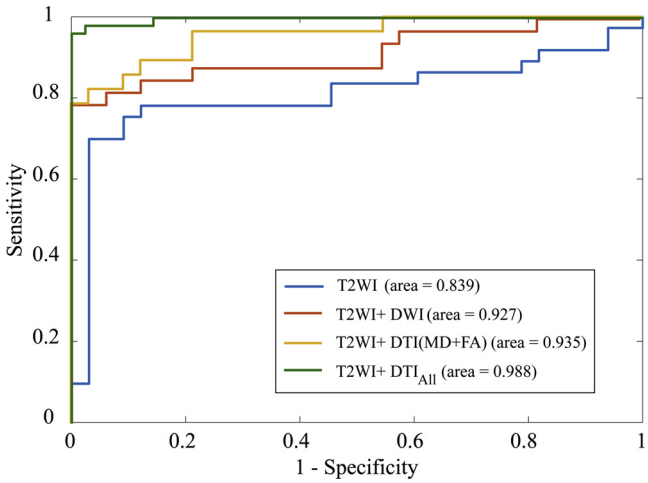

Fig. 4. Receiver Operating Characteristic (ROC) curves illustrating the diagnostic ability of T2WI, T2WI + DWI, T2WI + DTI(combined MD and FA) and T2WI + DTI$_{All}$ (combined statistically significant DTI parameters (p-value < 0.05)) for discrimination of cancer and healthy tissues. The area under ROC curve significantly increased (+5.70%) upon using combined DTI quantitative parameters (p-value < 0.05).

2.4. Image analysis

T2WI, DWI and DTI were exported from Siemens *syngo* in DICOM format. There is no consensus over workflow for prostate DTI post-processing. In this study, we used a basic and time-efficient post-processing approach (~10 min per patient). Eddy current correction and motion correction was performed using the "correct for subject motion & eddy current (EC) distortion" tool within the ExploreDTI software (ExploreDTI V.4.8.3, http://www.ExploreDTI.com) [21]. For noise reduction, an adaptive anisotropic diffusion filter was performed using the log-Euclidean anisotropic filter available from the software package, MedINRIA [22]. The filtered tensor images were imported into DTIStudio and used to generate eigen values (primary [λ_1], secondary [λ_2], and tertiary [λ_3]) [22]. Subsequently, these three eigenvalues served to calculate FA, RA, VR, C_l, C_p, C_s, AC, Mode, MD, RD, $\lambda_1 - \lambda_2$, $\lambda_1 - \lambda_3$, $\lambda_2 - \lambda_3$, VD, $S_{e_1e_2}$, $S_{e_1e_3}$ and $S_{e_2e_3}$ maps using Matlab 2015b software (Mathwork, USA).

All images and biopsy reports were individually assessed (by two experienced radiologists (one radiologist with more than twenty years' and one with twelve years' experience of prostate radiology). The

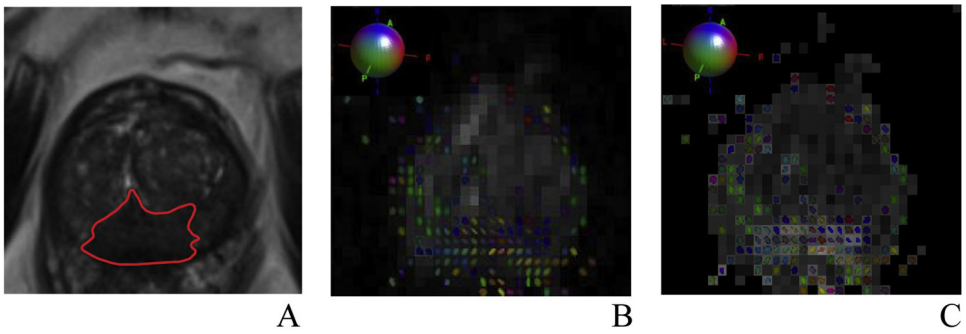

Fig. 5. A) Prostate T2WI of a 73-year-old man with a PSA value of 37.2 ng/mL and 4 + 5 Gleason score peripheral zone prostate cancer in left and right peripheral zone (PZ) prescribed (red line), B) color-coded fiber tract ellipsoids (glyph) derived from diffusion tensor in each image voxel overlaid on image with b-value = 0 s/mm^2 and C) fractional anisotropy (FA). Anisotropy map was color-coded according to principle direction of diffusion (red: right-left, green: anterior-posterior and blue: head-foot). The local diffusion variation in cancer area in B and C are much higher than other areas, as can be seen by variable orientation of ellipsoids.

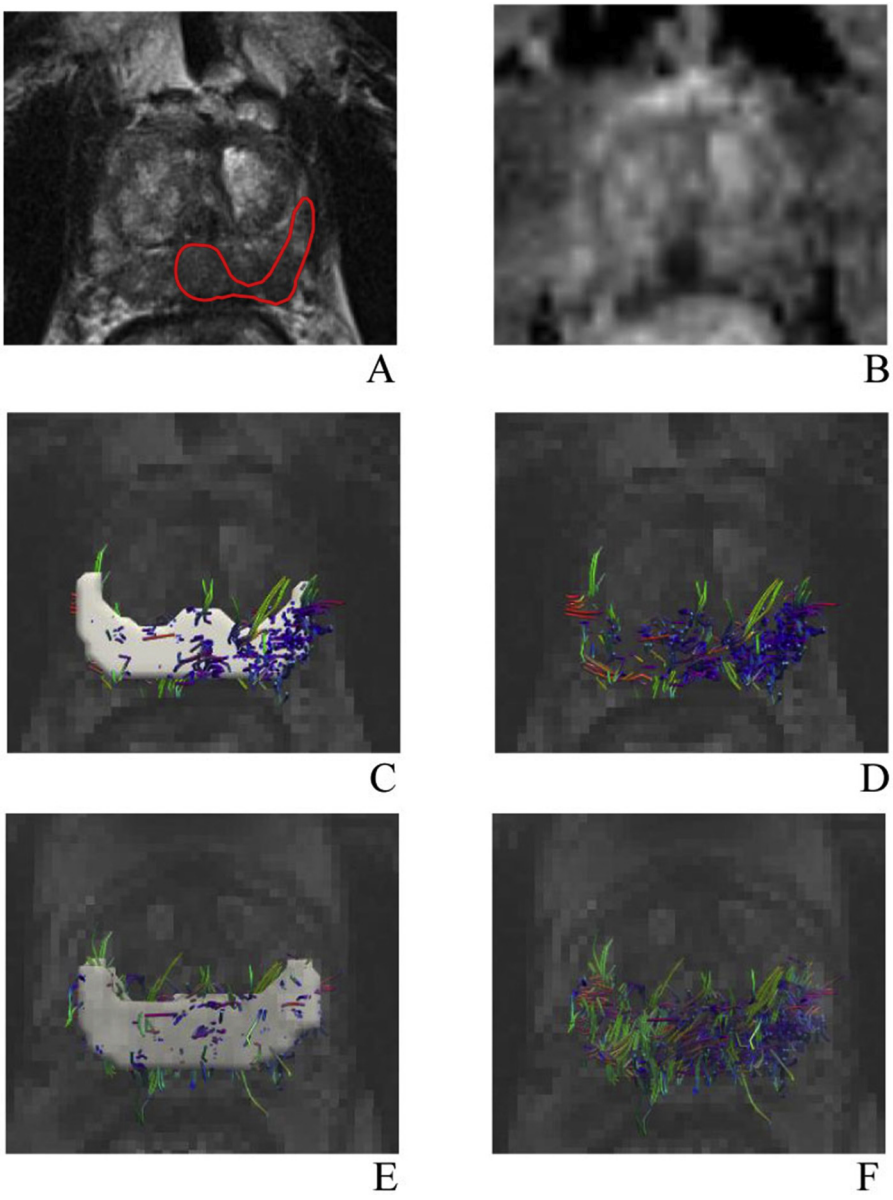

Fig. 6. A) T2WI of a 74-year-old man with a PSA value of 14.4 ng/mL and 4 + 5 Gleason score peripheral zone prostate cancer in the middle and left peripheral zone (PZ) with red color outline indicating cancer region of interest (ROI) and B) mean diffusivity (MD) map. C, D correspond to the visualization of fiber tract density for entire peripheral zone using DTI tractography derived from single slice. E, F correspond to the visualization of fiber tract density for entire peripheral zone using DTI tractography derived from five contiguous slices. Fiber tracts color-coded according to principle direction of diffusion (red: right-left, green: anterior-posterior and blue: head-foot).

biopsy pathology report was used as a gold standard. Radiologists visually matched apparent diffusion coefficient (ADC) map, baseline image (b-value = 0 s/mm^2), and corresponding T2WI slice locations and gland anatomy (apex, mid-gland area and base). After separate evaluation, the cancer ROIs were manually outlined by the radiologists in the peripheral zone (PZ) on T2WI and the baseline image using OsiriX software (OsiriX V.0.9.0, Pixmeo, Geneva, Switzerland). Concordance between the two radiologists was secured prior to quantitative analysis. The rest of PZ was used as healthy ROIs (In patients with benign cores, healthy ROIs were selected from non-cancer and non-benign areas by radiologists).

The feasibility for mapping of cancer and healthy fibrous anatomy

Table 3
Analysis of DTI metrics for two different Gleason scores and Spearman correlation coefficient with Gleason scores. Only DTI parameters with | r | > 0.25 are listed.

DTI Feature	Gleason Score		p-value	r*
	7	9		
FA	0.30 ± 0.04	0.34 ± 0.03	0.062	0.365
RA	0.15 ± 0.02	0.20 ± 0.02	< 0.001	0.657†
C_l	0.08 ± 0.01	0.11 ± 0.01	0.001	0.655†
C_p	0.18 ± 0.03	0.22 ± 0.01	0.013	0.389
C_s	0.73 ± 0.03	0.72 ± 0.06	0.211	−0.402
AC	0.23 ± 0.06	0.28 ± 0.07	0.028	0.383
λ_3 (× 10^{-3} mm^2/sec)	0.72 ± 0.12	0.60 ± 0.15	0.043	−0.332
RD (× 10^{-3} mm^2/sec)	0.86 ± 0.21	0.75 ± 0.11	0.062	−0.289
$S_{e_2e_3}$(× 10^{-3} mm^2/sec)^2	0.76 ± 0.24	0.59 ± 0.22	0.024	−0.341

Fractional anisotropy (FA), relative anisotropy (RA), volume ratio (VR), linear anisotropy (C_l), planar anisotropy (C_p), spherical anisotropy (C_s), attenuation coefficient (AC), orthogonal diffusivity to λ_1 (λ_3), radial diffusivity (RD) and surface diffusivity ($S_{e_2e_3}$).

† Strong positive correlation.

* correlation between combined Gleason scores and DTI feature.

was evaluated using DTI tractography, [14] which was performed using two open source software packages: Diffusion Toolkit version 0.6.4.1 and TrackVis version 0.6.1 (www.trackvis.org). An angle threshold of 60° was selected to reduce artefactual reconstructions. The baseline images and contours were imported to TrackVis software. The TrackVis software reports the number of fibers in each region after tract mapping. Then the total tract number in each region was divided by the volume of each segmented region [23] to calculate the average fiber tract density.

2.5. Statistical analysis

The mean values of the DTI parameters and the average number of fiber tract density were calculated from each cancerous and healthy ROI. The Mann Whitney U test using IBM SPSS software (SPSS V.0.24.0, Chicago, IL, USA) was used to compare the mean value of each ROI and the capability of the DTI metrics for differentiation between cancer and healthy tissues. Statistical significance was defined as p-value < 0.05. Diagnostic performance of DTI parameters were analysed with receiver operating characteristic (ROC). Youden indices were used for defining cutoff values of DTI parameters.

Four binary support vector machine (SVM) classifications with a radial basis function (RBF) kernel (RBF SVM) between healthy and cancer was developed using Matlab 2015b software. ROC curves were used to evaluate and compare the diagnostic performance of T2WI, T2WI + DWI, T2WI + DTI (MD + FA) and T2WI + DTI_{ALL} (all DTI quantitative parameters with a significant difference between the two groups (p-value < 0.05)).

The RBF SVM was defined by two parameters: misclassification cost (C) and inverse of support vector's radius of influence (γ). Optimal values of the parameters C and γ were calculated by performing a grid search of 2^{-5}, ..., 2^5 for C and 2^{-10}, ..., 2^{10} for γ and the best combination was selected for each classifier. Due to small sample size, a leave-one-out cross-validation was used to evaluate the performance of SVM classification models.

To determine the correlation of DTI parameters with tumour aggressiveness, the cancer data was divided into two groups (Gleason score 7 and Gleason score 9) and the same statistical analysis was used to measure the difference in DTI parameters between the two groups. Spearman correlation coefficient (r) was used to measure the correlation between combined Gleason score cohorts and each DTI parameter.

3. Results

Twenty-one 3D quantitative maps were generated from eleven prostate cancer patients. Clinical information of the patients is summarized in Table 1.

3.1. Quantitative DTI parameters in Cancer and healthy regions of interest

The MD map and new diffusivity maps generated from DTI are shown in Fig. 2. The dominant and suspicious lesions are more visible in VD, $S_{e_1e_2}$, $S_{e_1e_3}$ and $S_{e_2e_3}$ maps (Fig. 2C-F), and are more visually distinct from the surrounding tissue, compared to T2WI and MD maps (Fig. 2A-B). These new maps represent improvement over MD and T2WI. Fig. 3 shows a set of images/parametric maps generated from DTI data, with region of cancer delineated in red on T2WI by the radiologist. The border of PZ cancer lesion in AC and VD maps (Fig. 3D-E) is more obvious than T2WI and MD maps (Fig. 3A-B). Additionally, the corresponding cancer area on T2WI (Fig. 3A) is represented as brighter area than surrounding PZ tissue on FA and RA maps (Fig. 3C and Fig. 3F).

The total mean values of healthy and cancer ROIs and corresponding p-values from the DTI parameter maps were summarized in Table 2. These results indicate that all diffusivity parameters, except

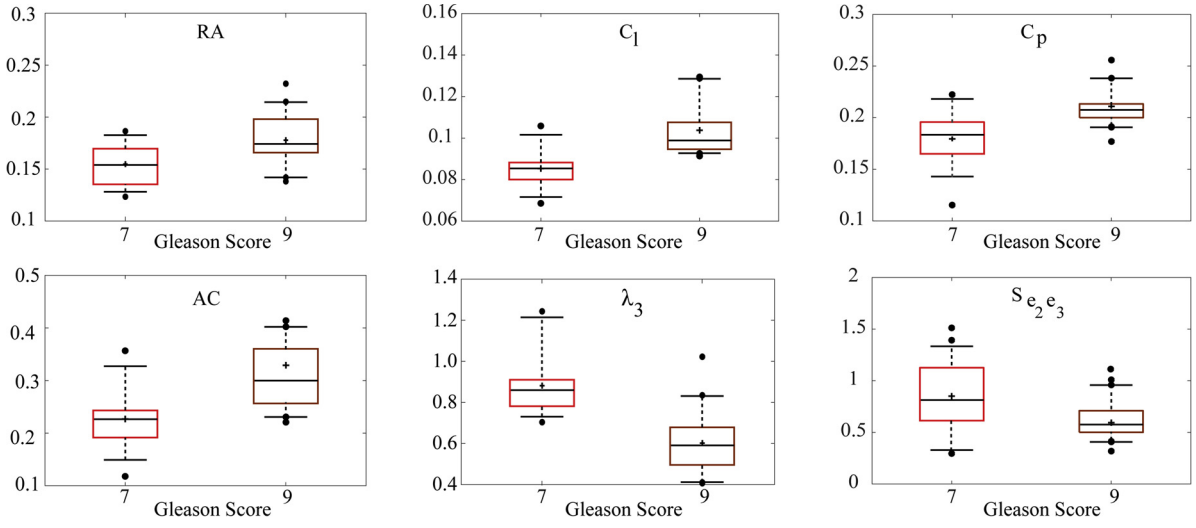

Fig. 7. Scatter and box plots of statistically significant DTI parameters (p-value < 0.05) for prostate Gleason scores (7 and 9). Notice that the diagnostic efficacy (difference of means) is highest for relatively anisotropy (RA) and linear anisotropy (C_l), as reflected by their correlation coefficients (> 0.6).

$\lambda_1 - \lambda_3$ and $\lambda_2 - \lambda_3$, and all anisotropy parameters, except Mode, have a statistically significant difference between cancer and healthy regions (p-value < 0.01). Additionally, mean fiber tract density obtained from DTI tractography in cancer regions was significantly higher than the corresponding mean in healthy regions (+38.22%, p-value < 0.05). Although there was variation in fiber tract densities among prostate cancer patients, DTI tractography depicts cancer regions containing higher average numbers of fiber tracts.

The ROC curve illustrated in Fig. 4 shows the diagnostic performance of T2WI, T2WI + DWI, T2WI + DTI(MD + FA) and T2WI + DTI_{All} for cancer and healthy tissues. The area under ROC curve of T2WI (95% confidence interval CI) = 0.839, range = 0.795-0.923, sensitivity/Specificity = 0.918/0.705) and T2WI + DWI (95% CI = 0.927, range = 0.875-0.990, sensitivity/Specificity = 0.938/0.902). The area under ROC curve performance of MD + FA classifier (95% CI = 0.935, range = 0.898-0.999, sensitivity/specificity = 0.957/0.917) improves (+5.70%) when other statistically significant DTI parameters are included (95% CI = 0.988, range = 0.975–1.00, sensitivity/specificity = 1.00/0.932, p-value < 0.05). These results indicate that combined statistically significant DTI parameters have a better capacity for discriminating cancer tissues from healthy tissues in PZ of the prostate.

Fig. 5B and Fig. 5C are the glyph-based visualization of the DTI overlaid with b-value = 0 and FA map in prostate tissue. These figures reveal local variation in diffusion tensor fields by mapping tensor properties to the ellipsoids (glyph), where the length of ellipsoid in a particular direction reflects magnitude of diffusion in that particular direction. These ellipsoids disappeared in isotropic regions showing more isotropic structures [24,25]. These figures illustrate the anisotropic variation of cancer and healthy tissues in the prostate and can be used to monitor the structural tissue dynamics.

An example of the DTI tractography in the PZ prostate is shown in Fig. 6. This figure shows the capability of DTI tractography to evaluate fiber tract density of the cancer and healthy prostate regions derived from prostate DTI. This figure shows DTI tractography of PZ for single slice (Fig. 6C, D) and five contiguous slices (Fig. 6E, F). The single slice allows better visualization of the tract density in cancer and healthy regions. However, the multiple slice results were used to measure tract density of cancer and healthy regions for each patient. For this particular patient, the volume of the peripheral zone, cancer and healthy regions from five slices were 14.17 ml, 5.79 ml and 8.38 ml, respectively. The corresponding tract number for the peripheral zone tracts, cancer region tracts and healthy region tracts were 297, 161 and 136, respectively.

3.2. Correlation of DTI parameters with gleason score

Correlation coefficients of DTI parameters with Gleason score were calculated to determine whether these parameters can be used to predict aggressiveness of PZ prostate cancer. The total mean values of the DTI metrics with correlation coefficient of $|r| > 0.25$ for two different Gleason scores, along with their respective p-values are summarized in Table 3.

These results demonstrated that C_l and RA had statistically significant and relatively strong positive correlations ($r > 0.60$, p-value < 0.001) with Gleason score, whereas other metrics had lower and medium correlations with Gleason scores ($0.25 < |r| < 0.5$). In spite of the low correlation of λ_3, S_{e2e3}, AC and C_p with Gleason score, λ_3 and S_{e2e3} significantly decreased and AC and C_p significantly increased with increasing Gleason scores (p-value < 0.05). However, correlation coefficient for other DTI parameters including fiber tract density derived from DTI tractography with Gleason score were low and non-significant ($|r| < 0.25$, p-value > 0.05).

Fig. 7 shows a boxplot representing the most statistically significant DTI parameters between Gleason scores of 7 and 9 (p-value < 0.05), highlighting the diagnostic capabilities of C_l and RA.

4. Discussion

DTI provides valuable information about microstructural properties of many tissues, including prostate [11,12,15]. There has been an increasing interest in utilizing high b-value diffusion MRI to improve the specificity of high-grade prostate cancer detection despite their lower SNR [20]. In this study, a b-value of 1600s/mm^2 was used to improve specificity of cancer detection. However, *in vivo* and simulation-based brain studies reported an upward bias of FA and no significant bias in MD as SNR decreased [26]. There is evidence to suggest that a higher number of gradient directions increases SNR of DTI [19]. In this study, we acquired high quality prostate DTI in thirty different gradient directions to improve SNR without endorectal coil [27,28]. Furthermore, using higher number of diffusion gradient directions, novel diffusivities and tractography parameters and anisotropy maps were generated and evaluated to assess lesion aggressiveness and diagnostic potential [29].

Most prostate DTI studies emphasized on MD and FA parameters in cancer and healthy tissues [30,31]. These studies suggested that the MD values decrease in tumours, while the FA decrease, increase or invariant in prostate tumours [11,12,32,33]. In a 3 T study, Gürses et al. found that mean FA of TRUS-proven cancer was significantly higher than FA of chronic prostatitis and normal tissue [11]. They also found that the mean ADC of cancerous tissue was significantly lower than non-cancerous tissues. However, no significant difference between MD and FA values of prostatitis and normal prostate was detected [11]. This agreed with Li et al. who reported increased FA and decreased MD in PZ prostate cancer at 3 T [32]. This partially contradicted findings by Manenti et al. who detected significant decrease in MD and FA values in biopsy proven PZ prostate cancer compared to healthy areas at 3 T [33]. In a separate 3 T study, Nezzo et al. reported a negative correlation between MD and Gleason score and no correlation between FA and Gleason score [12]. This discrepancy in FA correlation with prostate cancer might be explained by acquisition protocol parameters and/or post-processing techniques (directions, b-value, etc.) [20,28].

. The FA and MD values from the current study were similar to the results of other studies in PZ with a larger number of patients [33]. Only Sinha et al. evaluated the tensor but only in normal tissues [31]. Our results yielded lower diffusivity and higher anisotropy values of cancer tissues from multiple DTI maps suggesting more structured or packed organization of cancer cells and/or tissue [34]. This study also investigated four novel quantitative DTI parameters for prostate cancer detection, namely; volume diffusivity and three surface diffusivity maps. These four parameters offered improved visualization of tumour margins and prostate cancer tissue characterization over other diffusivity and anisotropy DTI maps. These new parameters and other diffusivity and anisotropy DTI based maps introduced in this paper may provide additional information for the clinical assessment of prostate cancer. In addition, the decreased diffusivity parameters and increased anisotropy parameters indicate that barriers, cell membrane and complex fiber networks increase in cancer compared to healthy tissues [9,10].

DTI tractography analysis was performed for fiber characterization and micro-architecture of prostate tissue *in vivo*. In spite of the conservative number of patients used, a statistically significant increase in fiber tract density was detected. This agrees with increased neuronal fiber density findings in prostate cancer biopsies and their association with aggressive cancer as reported elsewhere [4,35]. In addition, as nerve fibers in prostate cancer induce an angiogenic switch, [7] blood vessel density is also increased and may contribute, along with increased nerve density, to our observation that fiber tract density is increased in cancer compared to healthy region of the prostate. These quantitative features have made it possible to detect pathology-specific details such microstructural changes of prostate tissues.

To our knowledge none of the previous studies combined novel diffusivity parameters, anisotropic DTI features, and tract density of DTI tractography. Also, this is the first study demonstrating the role of

DTI and DTI tractography for characterization of the prostate cancer with perineural invasion.

The AUC of the statistically significant DTI parameters demonstrated the capability for the discrimination of cancer and healthy ROIs (AUC (%95 CI) = 0.988, range = 0.975–1.00). Our results suggest that DTI selected parameters and fiber tract density of tractography has the potential to improve prostate cancer characterization. For this purpose, DTI might be considered as a third acquisition technique in addition to T2WI in a multi-parametric MRI examination of the prostate. However, the diagnostic performance of T2WI + DTI(MD + FA) was slightly higher than T2WI + DWI (+0.86%).

A negative correlation between diffusivity parameters and Gleason score have been predicted using a reliable model [36] and is supported by RD, λ_3 and $S_{e_2e_3}$ parameters in our investigation. Variation in the tissue architecture in aggressive prostate cancer, which occurs with the replacement of low cellular density normal tissue with highly cellular neoplastic tissue, results in more restricted movement of water molecules [37]. In our investigation of the relationship between the anisotropy parameters and Gleason score, we found that there is a strong positive correlation of RA and Gleason score indicating that in tissue with higher Gleason score, anisotropic contribution is becoming more dominant. In addition, the observed significant increase in linear and planar anisotropy (C_l and C_p) is probably due to internal structural transformation from a spherical (no alignment) to a more cigar and/or disc shaped diffusion ellipsoid structure (increased alignment) [34,38]. The above finding is also supported by the strong positive correlation between linear anisotropy (C_l) and Gleason score. This result might suggest that water diffusion is becoming more restricted due to the increased tumor cellularity which agrees with *ex vivo* onset of nerve infiltration (neurogenesis) in prostate cancer [39,40].

However, the measured fiber tract density, did not yielded a statistically significant difference between Gleason score 7 and 9 (p-value = 0.158). This can be explained by low variability in cell density and the small number of samples used in either group of Gleason scores [37].

DTI and DTI fiber tractography enable the identification of characteristic micro-structural details of tissue in vivo. DTI has the potential to be used as an adjunct to conventional MRI in daily clinical practice as a predictor of suspicious PIRADS 3–5 lesions, recurrence likelihood and, extra-prostatic extension and thus can be of prognostic utility. Furthermore, DTI parameters has the potential to DTI parameters improve the prognostic stratification of the individual patient and to offer new personalized planning for high-risk patients.

A limitation of the study is the low number of patients, however, the number of prostate cancer patients with perineural invasion is quite low.

5. Conclusion

This study presents a more detailed analysis of DTI and DTI tractography for human PZ prostate cancer with perineural invasion. The results show that quantitative parameters of DTI have the potential to improve prostate cancer identification and characterization. These parameters appear to be a promising tool for evaluating the pathological changes of prostate cancer tissue, such as predict pathologic stage of the tumor. More importantly, DTI tractography seems to be suited for structural studies in prostate cancer and was in agreement with increased neuronal tract density reported in prostate cancer. This information might be useful for evaluating recurrence and guiding accurate nerve-sparing radical prostatectomy. Further studies on the impact of DTI and DTI tractography on diagnostic and prognostic factors are required to verify our preliminary findings.

Grant support

This study was supported by the Hunter Cancer Research Alliance (HCRA), NSW, Australia [Grant number: G1301098, 2015].

Conflict of interest

N. Gholizadeh, P.B Greer, J. Simpson, J. Denham, P. Lau, J. Dowling, H. Hondermarck and S. Ramadan declare that they have no conflict of interest.

Acknowledgements

This research was supported by the Imaging Centre of the University of Newcastle and Calvary Mater Newcastle. We would especially like to acknowledge the contribution of the Clinical Research and Statistical Support unit in Hunter Medical Research Institute (HMRI).

References

[1] Australian Institute of Health and Welfare and Australasian Association of Cancer Registries, (AIHW), Cancer in Australia: An Overview 2014, AIHW Catalogue no CAN 88 Cancer Series no 90, (2014), p. 71.
[2] G.E. Ayala, H. Dai, M. Ittmann, R. Li, M. Powell, A. Frolov, T.M. Wheeler, T.C. Thompson, D. Rowley, Growth and survival mechanisms associated with perineural invasion in prostate cancer, Cancer Res. 64 (17) (2004) 6082–6090.
[3] B. Boilly, S. Faulkner, P. Jobling, H. Hondermarck, Nerve dependence: from regeneration to Cancer, Cancer Cell 31 (3) (2017) 342–354.
[4] C. Magnon, S.J. Hall, J. Lin, X. Xue, L. Gerber, S.J. Freedland, P.S. Frenette, Autonomic nerve development contributes to prostate cancer progression, Science 341 (6142) (2013) 1236361.
[5] J. Pundavela, Y. Demont, P. Jobling, L.F. Lincz, S. Roselli, R.F. Thorne, D. Bond, R.A. Bradshaw, M.M. Walker, H. Hondermarck, ProNGF correlates with Gleason score and is a potential driver of nerve infiltration in prostate cancer, Am. J. Pathol. 184 (12) (2014) 3156–3162.
[6] A. Olar, D. He, D. Florentin, Y. Ding, G. Ayala, Biologic correlates and significance of axonogenesis in prostate cancer, Hum. Pathol. 45 (7) (2014) 1358–1364.
[7] A.H. Zahalka, A. Arnal-Estapé, M. Maryanovich, F. Nakahara, C.D. Cruz, L.W. Finley, P.S. Frenette, Adrenergic nerves activate an angio-metabolic switch in prostate cancer, Science 358 (6361) (2017) 321–326.
[8] K. Kitajima, S. Takahashi, Y. Ueno, H. Miyake, M. Fujisawa, F. Kawakami, K. Sugimura, Do apparent diffusion coefficient (ADC) values obtained using high b-values with a 3-T MRI correlate better than a transrectal ultrasound (TRUS)-guided biopsy with true Gleason scores obtained from radical prostatectomy specimens for patients with prostate cancer? Eur. J. Radiol. 82 (8) (2013) 1219–1226.
[9] P. Mukherjee, J.I. Berman, S.W. Chung, C.P. Hess, R.G. Henry, Diffusion Tensor MR Imaging and Fiber Tractography: Theoretic Underpinnings, Am. J. Neuroradiol. 29 (4) (2008) 632–641.
[10] W. Van Hecke, L. Emsell, S. Sunaert, Diffusion Tensor Imaging: A Practical Handbook, Springer, 2015.
[11] B. Gürses, N. Tasdelen, F. Yencilek, N.O. Kılıckesmez, T. Alp, Z. Fırat, M.S. Albayrak, A.M. Uluğ, A.N. Gürmen, Diagnostic utility of DTI in prostate cancer, Eur. J. Radiol. 79 (2) (2011) 172–176.
[12] M. Nezzo, M.G. Di Trani, A. Caporale, R. Miano, A. Mauriello, P. Bove, S. Capuani, G. Manenti, Mean diffusivity discriminates between prostate cancer with grade group 1&2 and grade groups equal to or greater than 3, Eur. J. Radiol. 85 (10) (2016) 1794–1801.
[13] L. Jiang, C.-Y. Xiao, Q. Xu, J. Sun, H. Chen, Y.-C. Chen, X. Yin, Analysis of DTI-Derived tensor metrics in differential diagnosis between low-grade and high-grade gliomas, Front. Aging Neurosci. 9 (271) (2017).
[14] D.S. Finley, B.M. Ellingson, S. Natarajan, T.M. Zaw, S.S. Raman, P. Schulam, R.E. Reiter, D. Margolis, Diffusion tensor magnetic resonance tractography of the prostate: feasibility for mapping periprostatic fibers, Urology 80 (1) (2012) 219–223.
[15] V. Panebianco, F. Barchetti, A. Sciarra, A. Marcantonio, C. Zini, S. Salciccia, F. Collettini, V. Gentile, B. Hamm, C. Catalano, In vivo 3D neuroanatomical evaluation of periprostatic nerve plexus with 3T-MR Diffusion Tensor Imaging, Eur. J. Radiol. 82 (10) (2013) 1677–1682.
[16] S. Mori, Chapter 4 - Principle of Diffusion Tensor Imaging, Introduction to Diffusion Tensor Imaging, Elsevier Science B.V., Amsterdam, 2007, pp. 33–40.
[17] S. Mori, J. Zhang, Principles of diffusion tensor imaging and its applications to basic neuroscience research, Neuron 51 (5) (2006) 527–539.
[18] R. Shimofusa, H. Fujimoto, H. Akamata, K. Motoori, S. Yamamoto, T. Ueda, H. Ito, Diffusion-weighted imaging of prostate cancer, J. Comput. Assist. Tomogr. 29 (2) (2005) 149–153.
[19] N. Zhang, Z.-S. Deng, F. Wang, X.-Y. Wang, The effect of different number of diffusion gradients on SNR of diffusion tensor-derived measurement maps, J. Biomed. Sci. Eng. 2 (02) (2009) 96.
[20] H.K. Agarwal, F.V. Mertan, S. Sankineni, M. Bernardo, J. Senegas, J. Keupp, D. Daar, M. Merino, B.J. Wood, P.A. Pinto, P.L. Choyke, B. Turkbey, Optimal high b-value for diffusion weighted MRI in diagnosing high risk prostate cancers in the peripheral zone, J. Magn. Reson. Imaging 45 (1) (2017) 125–131.
[21] J. Soares, P. Marques, V. Alves, N. Sousa, A hitchhiker's guide to diffusion tensor

imaging, Front. Neurosci. 7 (2013) 31.
[22] S. Sinha, U. Sinha, V. Malis, V. Bhargava, K. Sakamoto, M. Rajasekaran, Exploration of male urethral sphincter complex using diffusion tensor imaging (DTI)-based fiber-tracking, J. Magn. Reson. Imaging (2018).
[23] I. Karademir, D. Shen, Y. Peng, S. Liao, Y. Jiang, A. Yousuf, G. Karczmar, S. Sammet, S. Wang, M. Medved, T. Antic, S. Eggener, A. Oto, Prostate volumes derived from MRI and volume-adjusted serum prostate-specific antigen: correlation with Gleason score of prostate cancer, AJR Am. J. Roentgenol. 201 (5) (2013) 1041–1048.
[24] P. Kondratieva, J. Kruger, R. Westermann, The application of GPU particle tracing to diffusion tensor field visualization, Visualization, 2005. VIS 05. IEEE (2005) 73–78.
[25] T. McGraw, B.C. Vemuri, Y. Chen, M. Rao, T. Mareci, DT-MRI denoising and neuronal fiber tracking, Med. Image Anal. 8 (2) (2004) 95–111.
[26] J.A.D. Farrell, B.A. Landman, C.K. Jones, S.A. Smith, J.L. Prince, P.C.M. van Zijl, S. Mori, Effects of SNR on the accuracy and reproducibility of DTI-derived fractional anisotropy, mean diffusivity, and principal eigenvector measurements at 1.5T, J. Magn. Reson. Imaging 26 (3) (2007) 756–767.
[27] C. Shenhar, H. Degani, Y. Bar, J. Baniel, S. Tamir, O. Binyaminov, E. Furman-Haran, D. Margel, Innovative diffusion MRI protocol to improve prostate cancer diagnosis, Eur. Urol. Suppl. 17 (2) (2018) e1883–e1884.
[28] D.K. Jones, The effect of gradient sampling schemes on measures derived from diffusion tensor MRI: a Monte Carlo study, Magnet. Reson. Med. 51 (4) (2004) 807–815.
[29] L. Zhan, M.-C. Chiang, M. Barysheva, A.W. Toga, K.L. McMahon, G.I. de Zubicaray, M. Meredith, M.J. Wright, P.M. Thompson, How many gradients are sufficient in high-angular resolution diffusion imaging (HARDI), Workshop on Computational Diffusion MRI, MICCAI (2008) 216–224.
[30] P. Gibbs, M.D. Pickles, L.W. Turnbull, Diffusion imaging of the prostate at 3.0 tesla, Invest. Radiol. 41 (2) (2006) 185–188.
[31] S. Sinha, U. Sinha, In vivo diffusion tensor imaging of the human prostate, Magn. Reson. Med. 52 (3) (2004) 530–537.
[32] L. Li, D.J. Margolis, M. Deng, J. Cai, L. Yuan, Z. Feng, X. Min, Z. Hu, D. Hu, J. Liu, L. Wang, Correlation of gleason scores with magnetic resonance diffusion tensor imaging in peripheral zone prostate cancer, J. Magn. Reson. Imaging 42 (2) (2015) 460–467.
[33] G. Manenti, M. Carlani, S. Mancino, V. Colangelo, M. Di Roma, E. Squillaci, G. Simonetti, Diffusion tensor magnetic resonance imaging of prostate cancer, Invest. Radiol. 42 (6) (2007) 412–419.
[34] C.F. Westin, S.E. Maier, H. Mamata, A. Nabavi, F.A. Jolesz, R. Kikinis, Processing and visualization for diffusion tensor MRI, Med. Image Anal. 6 (2) (2002) 93–108.
[35] A. Olar, D. He, D. Florentin, Y. Ding, G. Ayala, Biologic correlates and significance of axonogenesis in prostate cancer, Hum. Pathol. 45 (7) (2014) 1358–1364.
[36] N. Gilani, P. Malcolm, G. Johnson, A model describing diffusion in prostate cancer, Magn. Reson. Med. 78 (1) (2017) 316–326.
[37] C.A. Woodfield, G.A. Tung, D.J. Grand, J.A. Pezzullo, J.T. Machan, J.F. Renzulli, Diffusion-weighted MRI of peripheral zone prostate cancer: comparison of tumor apparent diffusion coefficient with Gleason score and percentage of tumor on core biopsy, Am. J. Roentgenol. 194 (4) (2010) W316–W322.
[38] C.F. Westin, F. Szczepankiewicz, O. Pasternak, E. Ozarslan, D. Topgaard, H. Knutsson, M. Nilsson, Measurement tensors in diffusion MRI: generalizing the concept of diffusion encoding, Med. Image Comput. Comput. Assist. Interv. 17 (Pt 3) (2014) 209–216.
[39] K. Kitajima, S. Takahashi, Y. Ueno, H. Miyake, M. Fujisawa, K. Sugimura, Visualization of periprostatic nerve fibers before and after radical prostatectomy using diffusion tensor magnetic resonance imaging with tractography, Clin. Imaging 38 (3) (2014) 302–306.
[40] J.V. Hajnal, M. Doran, A.S. Hall, A.G. Collins, A. Oatridge, J.M. Pennock, I.R. Young, G.M. Bydder, MR imaging of anisotropically restricted diffusion of water in the nervous system: technical, anatomic, and pathologic considerations, J. Comput. Assist. Tomogr. 15 (1) (1991) 1–18.